THE JOURNAL OF PHYSICAL CHEMISTRY B

Article

pubs.acs.org/JPCB

Molecular Dynamics Investigation into Substrate Binding and Identity of the Catalytic Base in the Mechanism of Threonyl-tRNA Synthetase

Eric A. C. Bushnell,[†] WenJuan Huang,[†] Jorge Llano,[‡] and James W. Gauld*,[†]

[†]Department of Chemistry and Biochemistry, University of Windsor, Windsor, Ontario N9B 3P4, Canada

[‡]Department of Physical Sciences, Grant MacEwan University, Edmonton, Alberta T5J 4S2, Canada

ABSTRACT: The structure and nature of the fully bound active site of Threonyl-tRNA Synthetase (ThrRS) for the second half-reaction has been investigated using molecular dynamics simulations. More specifically, we examined the ThrRS active site with both the substrate Threonyl-AMP and the cosubstrate cognate Threonyl-tRNA bound. Furthermore, we also considered the cases in which an active-site histidyl residue (His309) is either neutral or protonated. Moreover, we considered the role a water molecule may play in formation of a viable Michaelis complex. From the results it is found that the most likely role of His309 is in binding and properly orientating the ribose of the Ado76 nucleotidyl residue of the threonyl-tRNA via formation of a direct His309···Ado76 hydrogen bond, i.e., without involvement of a water. In addition, the imidazole of the His309 residue is likely neutral. It was found that upon protonation the positioning of the Ado76-3′-OH was perturbed, leading to a reduced chance for nucleophilic attack of the threonyl's C1 center.

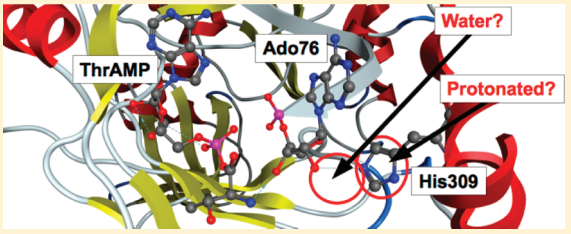

INTRODUCTION

Aminoacyl-tRNA synthetases (aaRS's) are ubiquitous in nature with central roles in a range of physiological processes including apoptosis, inflammation, and porphyrin biosynthesis.[1,2] They are perhaps most well known, however, for their critical role in protein biosynthesis. More specifically, they catalyze the activation of amino acids and attachment to their cognate tRNA.[2] The amino acid residues can then be polymerized by the cell's ribosomes to produce the genetically encoded proteins. For each of the 20 standard α-amino acids there exists a respective aaRS.[3] While differing in structure and having a low degree of sequence similarity, they do exhibit a number of commonalities.[2−10] In particular, the overall tRNA aminoacylation process as catalyzed by all aaRS's proceeds via two half-reactions. In the first, they catalyze the reaction of their specific target amino acid with adenosine triphosphate (ATP) to give the corresponding aminoacyl-adenylate (aaAMP) derivative with release of pyrophosphate (PP_i). In the second half, aaRS's catalyze the transfer of the aminoacyl (aa) group from the aaAMP to the 2′- or 3′-position of ribose of the cognate tRNA ($tRNA^{aa}$) at the Ado76 nucleotidyl residue (aa-$tRNA^{aa}$).[2,11,12]

Typically, in class I aaRS's, aminoacylation occurs at the Ado76-2′-oxygen and in class II at the Ado76-3′-oxygen. For both classes, however, it has been proposed that this process occurs via similar mechanisms (Scheme 1).[9,13] Specifically, a base within the active site is thought to deprotonate the target hydroxyl of the ribose sugar of the Ado76 residue. This enhances the nucleophilicity of the hydroxyl's oxygen and facilitates its attack at the carbonyl carbon of the amino acid moiety of the aaAMP substrate. In general, however, the exact identity of the Brønsted base is unclear. Indeed, the active sites of aaRS's typically lack any residue that may act as a proton acceptor in the esterification process.[13,14] In some cases, the basic group appears to be a nonbridging phosphate oxygen of the aaAMP substrate itself.[13,15] In a recent detailed computational study on a histidyl-RNA synthetase (HisRS),[16] we showed that it was thermodynamically feasible for the *pro-S* nonbridging phosphate oxygen to act as the required mechanistic base. In fact, it has been suggested[10] that such a substrate-assisted catalytic process may be a common approach in aaRS's.[10,13,17]

In the case of the class II threonyl-tRNA synthetase (ThrRS), however, recent mutagenesis studies by Minajigi and Francklyn[14] suggested that the aminoacyl-adenylate substrate's phosphate is *not* essential to the mechanism. In fact, only small decreases in the rate of reaction by no more than 3-fold were observed upon substitution of either the *pro-R* or the -*S* nonbridging phosphate oxygens. In contrast, substitution of an active-site histidine (His309) by alanine had a significantly larger effect, decreasing the reaction rate by ∼240-fold.[14] Hence, it was proposed that His309 may be the mechanistic base and, furthermore, that it may directly or indirectly (via a water molecule) deprotonate the Ado76-2′-OH group of the cognate tRNA ($tRNA^{Thr}$), which then subsequently deprotonates the adjacent Ado76-3′-OH group (Scheme 2).[14] Notably, for HisRS, substitution of the His-AMP substrate's *pro-S*

Received: March 16, 2012
Revised: April 5, 2012
Published: April 5, 2012

dx.doi.org/10.1021/jp302556e | *J. Phys. Chem. B* 2012, 116, 5205−5212

Scheme 1. Aminoacyl Transfer from aa-AMP to Ado76-3′-OH (second half-reaction) As Catalyzed by a Class II aaRS

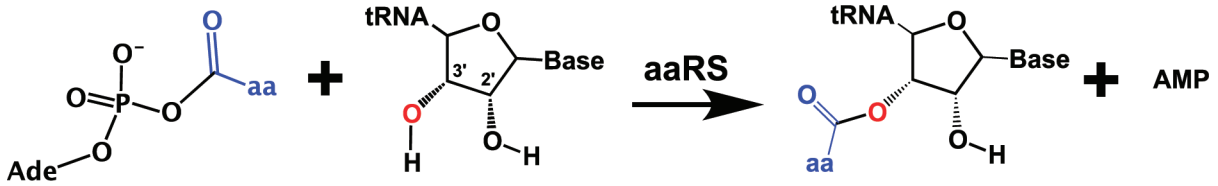

Scheme 2. Proposed Mechanism for Aminoacyl Transfer As Catalyzed by ThrRS via Deprotonation of 2′-OH-Ribonucleoside by His309[14]

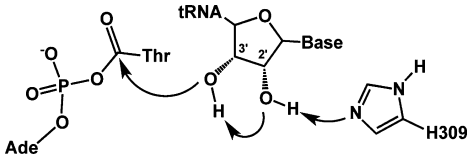

oxygen resulted in a considerably more marked rate decrease of ~10^4-fold.[17]

An important step in any enzymatic reaction is formation of a fully reactive enzyme–substrate complex, that is, the binding and positioning of substrate(s) and active-site functional groups, e.g., residues, cofactors, and water molecules. In addition, the structure of such complexes can provide invaluable insights into the catalytic pathway of that enzyme such as the identity of possible key active site functional groups and their potential mechanistic roles. To date, unfortunately, no experimentally derived NMR or X-ray structure for ThrRS has been reported in which both substrates for the second half-reaction (ThrAMP and $tRNA^{Thr}$) are bound within its active site.

Several X-ray crystallographic structures have been obtained, however, in which a substrate or substrate analogues are bound within the active site of ThrRS.[18−21] In particular, several structures have been obtained in which only the substrate analogues ThrAMS[19−21] (Figure 1a) or SerAMS[18] are bound, while another has been obtained[20] with both AMP *and* Thr-$tRNA^{Thr}$ simultaneously bound (Figure 1b). From these structures it was concluded that the aminoacyl-adenylate substrates *pro-R* and *-S* nonbridging oxygens likely interact with an arginyl and asparagyl residue, respectively. In addition, its aminoacyl moieties α-amino and side-chain hydroxyl (γ-OH) groups are bound to an active site Zn(II) ion (Figure 1a). This bidentate coordination has been proposed to be an essential characteristic of ThrRS, allowing the enzyme to discriminate against valine, which is the isosteric analog of threonyl.[21] It should be noted that on binding Thr a Zn(II)-bound water is displaced but may remain within the fully bound active site, as a water was detected in several crystallographic structures.[18−21] In addition, the Ado76-2′-OH group of the Thr-$tRNA^{Thr}$ moiety is thought to interact with the side chains of tyrosyl (Tyr462) and histidyl (His309), Figure 1b. The Tyr462···2′-OH interaction has been suggested to be important in binding of Thr-$tRNA^{Thr}$ to ThrRS. In particular, a peptide loop containing Tyr462 undergoes a conformational change, forming a hydrogen bond between the two groups. This resulting interaction is thought to help stabilize the active-site region by enabling formation of additional interactions, such as stacking of the highly conserved Phe461 and Asn312 residues.[21]

Computational methods are now widely applied in the study of enzyme chemistry including, for example, the structure and properties of enzyme–substrate/intermediate complexes.[22] In particular, it is noted that molecular dynamics (MD) methods have successfully been applied previously to the study of various aspects of aaRS chemistry.[15,23−31]

In this present study, MD simulations have been used to investigate the structure of viable Michaelis complexes for the enzyme ThrRS with both $tRNA^{Thr}$ and ThrAMP bound within its active site, i.e., complexes that would lead to aminoacyl transfer in the second half-reaction. In particular, we examined the effects of both a neutral and a protonated His309-N^{ϵ} side chain. Moreover, we considered the possible involvement of an active-site water in bridging between His309-N^{ϵ} and Ado76-2′-OH, thus acting as a proton shuttle in the deprotonation of the latter.[14]

COMPUTATIONAL METHODS

The Molecular Operating Environment (MOE)[32] software package was used for all calculations.

Design of Chemical Model. It has been experimentally observed that conformational changes occur within the active site of ThrRS upon binding of the $tRNA^{Thr}$ cosubstrate.[29,33] Hence, an X-ray crystal structure of a ThrRS···$tRNA^{Thr}$+AMP complex (PDB ID 1QF6)[29,33] was used as the template structure. This structure was then manually modified using MOE in order to include the missing threonyl moiety. Specifically, threonyl was added to the AMP substrate and positioned in the active site in accordance with that observed in X-ray crystal structures of the enzyme–substrate analogue complexes ThrRS···ThrAMS (PDB ID 1EVL and 1NYQ),[14,18] ThrRS···SerAMS (PDB ID 1FYF),[18,19,21] and ThrRS···Thr

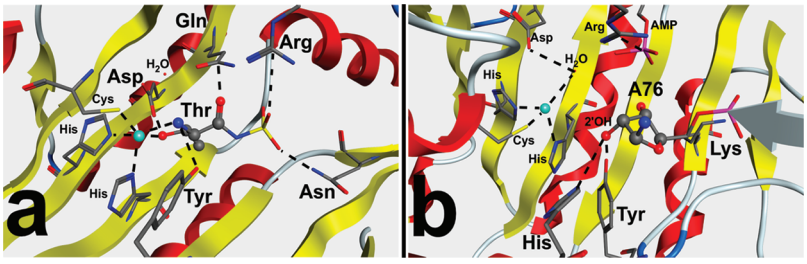

Figure 1. Active site of ThrRS bound with (a) Thr-AMP [PDB ID 1EVL][19] and (b) $tRNA^{Thr}$ and AMP [PDB ID 1QF6].[20]

dx.doi.org/10.1021/jp302556e | J. Phys. Chem. B 2012, 116, 5205−5212

(PDB ID 1NYR).[21] The α-NH_2 group of the Thr moiety (Thr-NH_2) and His309 residue were modeled as neutral.

Solvation and Annealing. Prior to data collection, an MD simulation was performed in order to obtain the corresponding solvated enzyme−substrates complex and enable it to undergo thermal relaxation. Specifically, the enzyme−substrate complex was surrounded by a 7 Å spherical layer of water molecules. An ellipsoidal potential wall with a scaling constant of 2 was then placed around the resulting solvated complex in order to force the system to lie within the volume of space defined by the ellipsoid. In addition, the distance between the 3′-OH and the C═O of the ThrAMP moiety was restrained by a force of 10 kcal mol^{-1} to a distance of 2.6 Å, thus allowing the whole system to reach a conformation consistent with the mechanistically relevant reactive conformation. It should be noted that this restraint was removed in all subsequent production runs. The damping functional factor included in the electrostatic and van der Waals potentials were set to decay smoothly beyond 8 and 10 Å. The geometry of the solvated complex was then optimized using the AMBER99 force field until the root-mean-square gradient of the total energy fell below 0.05 kcal mol^{-1} $Å^{-1}$.

The MD simulation was then performed under constrained pressure and temperature, while the equations of motion were coupled with the Nosé−Poincaré thermostat,[34] and the time step for numerical integration was set to 2 fs. The system was annealed by heating it from 150 to 300 K over a period of 25 ps, holding the temperature constant at 300 K for an additional period of 25 ps, then heating from 300 to 400 K over a period of 25 ps, and subsequently holding the temperature constant at 400 K for a further interval of 375 ps. At the 450 ps mark, the system was allowed to cool down by decreasing the temperature from 400 to 300 K over a period of 25 ps and then holding the temperature constant at 300 K for an interval of 25 ps.

Molecular Dynamics Production Runs. From the final structure of the above annealing simulation, four enzyme−substrate complexes were then obtained. The complexes differed in the protonation state of His309 and in the position of the water molecule in the vicinity of Ado76-2′-OH and His309 as a potential hydrogen-bond bridge between the two. The structure of each of the complexes was then optimized using the AMBER99 force field until the root-mean-square gradient of the total energy fell below 0.05 kcal mol^{-1} $Å^{-1}$. The damping functional factor included in the electrostatic and van der Waals potentials were set to decay smoothly beyond 8−10 Å. In addition, only those residues, nucleobases, and waters within 15 Å of the ThrAMP and Ado76 moieties were free to move, leaving all other atoms fixed at the positions that they ended up after the MD annealing. As described above for the annealing process, the subsequent MD simulations were performed under constrained pressure and temperature, the equations of motion were coupled with the Nosé−Poincaré thermostat,[34] and the time step for numerical integration was set to 2 fs. Each of the simulations was then run over 15 ns for equilibration, and the last 10 ns data of this equilibration phase were used for rmsd and cluster analyses.

RESULTS AND DISCUSSION

As detailed in the Introduction, aaRSs are thought to use a common catalytic approach for the second half-reaction. In particular, a base deprotonates either the Ado76-2′-OH or the Ado76-3′-OH hydroxyl group of the cognate tRNA cosubstrate. The resulting Ado76-2′-O^- or Ado76-3′-O^- oxyanion can then nucleophilically attack the carbonyl of the substrate aaAMP.[9,16] In contrast to that proposed for other aaRSs, in the case of ThrRS, an active site histidyl residue (His309) has been suggested to act as the catalytic base.[14] Specifically, its side-chain His309-N^{ε} center deprotonates the Ado76-2′-OH group either directly or via a bridging H_2O molecule. This is then followed by proton transfer from Ado76-3′-OH to the resulting Ado76-2′-O^- oxyanion (see Scheme 2). Within an aqueous environment at SATP, the pK_a of histidine's imidazole is approximately 6.0.[35] However, this value can significantly fluctuate under the influence of the local protein environment. For example, in aqueous solution at SATP, the pK_a of the guanidinium side chain of arginine is ∼12.5.[35] Yet, in the case of the enzyme UROD, we have previously shown that the reduced local polarity of its active-site environment markedly lowers the pK_a's of the R groups of two active-site arginyl residues such that they in fact may act as proton donors in the catalytic mechanism.[36]

Hence, since the aminoacyl transfer can potentially be either acid or base catalyzed, we considered the case of His309-N^{ε} being either protonated (His309-$N^{\varepsilon}H^+$) or neutral (His309-N^{ε}:) in the initial Michaelis complex. In the case of His309-$N^{\varepsilon}H^+$, the possible catalytic mechanism could involve transfer of the proton to the carbonyl oxygen of the ThrAMP substrate. This would enhance the electrophilicity of the adjacent carbonyl carbon center and thus, its susceptibility to nucleophilic attack by the Ado-3′-OH oxygen.

Accordingly, four models for the Michaelis complex of ThrRS, summarized in Table 1, were generated. We took into account that the water is either absent or present and that the His-N^{ε} center is either neutral (models **I** and **II**) or protonated (models **I**−$\mathbf{H}^+$ and **II**−$\mathbf{H}^+$). We also considered complexes in which the α-amine of the threonyl moiety was protonated. However, these led to structures that differed significantly from those experimentally obtained. A similar approach has recently been applied to investigate the structural dynamics of the riboswitch in the active site of glucosamine-6-phosphate synthetase with changing protonation states.[37] In particular, Banas et al.[37] carried out MD simulations involving various protonation states of three crucial active-site moieties to probe the dominant protonation states of these key active-site residues. In our investigation of each model of the Michaelis complex the root-mean-square deviations (rmsd's) in the positions of the His309 imidazole, Tyr462 phenol, Ado76 ribose ring, and the threonyl moiety were calculated over the last 10 ns of the production run. These rmsd's were calculated with respect to the minimized starting structure to ensure that the conformational equilibrium was reached. In the case of Model **II** and **II**−$\mathbf{H}^+$, the position of the bridging water was also included in rmsd calculation. Specifically, the phenol ring of Tyr462 was included because it has been suggested to be important in binding of ThrtRNA to ThrRS. As stated in the

Table 1. Summary of Michaelis Complex Models Considered in the Present Study

model	His309	Thr-NH_2	water
I	neutral	neutral	absent
I−$\mathbf{H}^+$	protonated	neutral	absent
II	neutral	neutral	present
II−$\mathbf{H}^+$	protonated	neutral	present

dx.doi.org/10.1021/jp302556e | J. Phys. Chem. B 2012, 116, 5205−5212

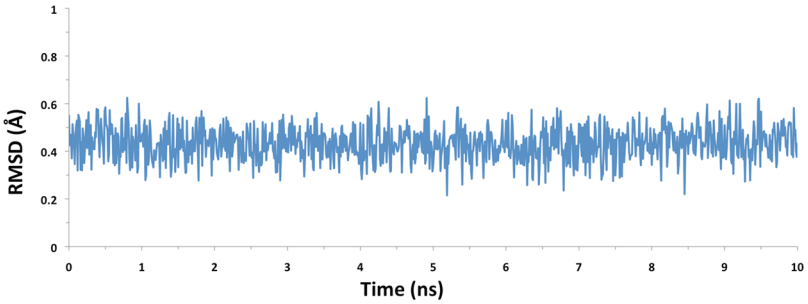

Figure 2. rmsd's in the positions of the imidazole of His309, phenol of Tyr462, ribose sugar ring of Ado76, and threonyl moiety during the 10 ns simulation of model **I**.

Introduction, a peptide loop containing Tyr462 undergoes a conformational change upon complete substrate binding such that the Tyr462-Ph−OH moiety forms a hydrogen bond to the Ado76-2′-OH group, with Tyr462 acting as the hydrogen-bond donor. This conformational change and resulting interaction is proposed to help stabilize the active-site region.[21]

Effects of Protonation at His309-N$^{\varepsilon}$ on Its Direct Hydrogen Bonding to Ado76-2′-OH. We began by considering the effects of protonating His309, specifically at its imidazole N$^{\varepsilon}$ center (His309-N$^{\varepsilon}$), on its hydrogen bonding with Ado76-2′-OH. For model **I** (i.e., neutral His309-N$^{\varepsilon}$ with no bridging H_2O) the rmsd's in the positions of the His309 imidazole, Tyr462 phenol, Ado76 ribose ring, and threonyl moiety relative to the optimized initial starting structure were calculated for each configuration obtained after equilibration during the production run (see Computational Methods). A plot of the calculated rmsd's is shown in Figure 2. As can be seen, during the production run the positions of the His309 imidazole, Tyr462 phenol, Ado76 ribose ring, and threonyl moiety maintain a quite consistent configuration. Indeed, with very few exceptions almost all rmsd's lie within a quite narrow range of 0.2−0.6 Å, indicating that there were no significant changes in their positions during the 10 ns production simulation.

The structures sampled during the simulation were investigated further using clustering analysis in order to group the rmsd's into five clusters. A representative average structure of each cluster was then selected, and their bound active sites were then overlaid with the others as shown in Figure 3.

As can be seen in Figure 3, the overlaid average structures show that within the fully abound active site a number of proposed mechanistically important interactions are quite consistent while some others appear to be more variable. For instance, in order to act as the required base as detailed in the Introduction, the His309 residue must obtain a proton from the Ado76-2′-OH group.[14] Over the 10 ns production run the 2′-H group is consistently positioned such that its proton is directed toward the neutral imidazole ε-nitrogen (N$^{\varepsilon}$) center of the His309 residue. Furthermore, it has an average His309-**N**$^{\varepsilon}$:···**O**-2′-Ado76 distance of 3.02 Å, which is only moderately shorter than observed experimentally (3.29 Å) in the available X-ray crystallographic structure (PDB ID 1QF6).[20] Similarly, a consistent Tyr462-O**H**···**O**-2′-Ado76 hydrogen-bonding interaction is also observed. Furthermore, it has an average Tyr462-**O**···**O**-2′-Ado76 distance of 2.88 Å, which is also in good agreement with that observed (2.81 Å) in the available X-ray crystallographic structure (PDB ID 1QF6).[20]

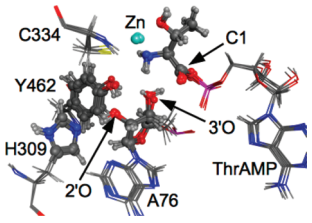

Figure 3. Overlay of the five representative average structures of model **I** obtained from cluster analysis of the rmsd's during the 10 ns MD production simulation. For clarity, not all hydrogens are shown. The enlarged atoms (except the Zn ion) are those used in calculation of the rmsd's presented in Figure 2. Color code: P, pink; C, gray; O, red; N, dark blue; S, yellow; Zn, light blue; H, white.

In contrast, considerably greater variability in the five average structures is observed for the orientation of the mechanistically key Ado76-3′-OH group. As detailed above (see Scheme 2), it has been proposed that the Ado76-2′-oxygen deprotonates the adjacent Ado76-3′-OH group.[14] However, over the course of the simulation only approximately 10.7% of the conformers obtained were observed to have a suitable orientation for a 2′-**O**···**H**-O-3′ hydrogen bond. Furthermore, during the 10 ns simulation, the 2′-**O**···**H**O-3′ distance varies quite significantly from 1.77 to 3.88 Å with a markedly long average distance of 3.11 Å. This elongated hydrogen-bond distance suggests that in model **I** (i.e., a neutral His309 residue and no additional active site water) it is unlikely that the Ado76-2′-oxygen would be able to deprotonate the adjacent Ado76-3′-OH group.

The effects of protonating His309 on the above fully bound active site were then examined using model **I**−**H**$^{+}$, i.e., His309-**N**$^{\varepsilon}$**H**$^{+}$ with no additional active site water. The rmsd's for the positions of the His309 imidazole, phenol of Tyr462, ribose ring of Ado76, and threonyl moiety relative to the starting structure were calculated for each structure and plotted in Figure 4. Similar to that observed above for the corresponding unprotonated fully bound active-site model **I**, overall, the positions of the above four moieties maintain a reasonably consistent configuration throughout the 10 ns simulation. However, the average rmsd is now moderately larger by approximately 0.2 Å, ranging from slightly below 0.4 Å to just over 0.8 Å (cf., Figure 2). This may indicate an increased mobility of the groups within the active site.

Cluster analysis was then performed on the rmsd's in Figure 4 to obtain five clusters. A representative average structure of each was then obtained and overlaid (Figure 5). As observed in the unprotonated fully bound active site (model **I**), all five structures have quite similar hydrogen-bonding networks. However, they also exhibit some key differences between each other and, importantly, from that observed in model **I**. For example, due to the fact that it is now protonated, the His309

dx.doi.org/10.1021/jp302556e | J. Phys. Chem. B 2012, 116, 5205−5212

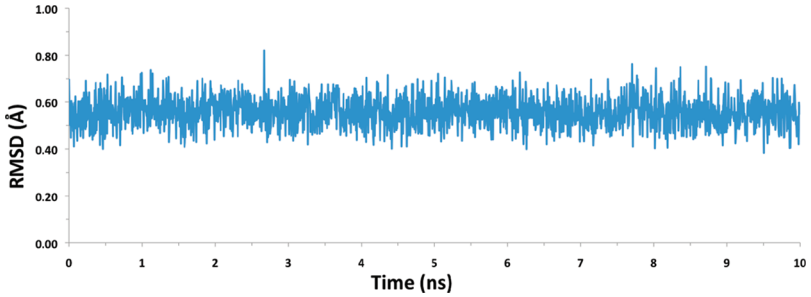

Figure 4. rmsd's in the positions of the imidazole of His309, phenol of Tyr462, ribose sugar ring of Ado76, and threonyl moiety during the 10 ns simulation of model **I**−**H**$^+$.

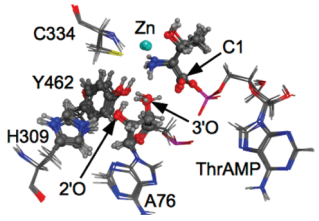

Figure 5. Overlay of the five representative average structures of model **I**−**H**$^+$ obtained from cluster analysis of the rmsd's during the 10 ns MD simulation. For clarity, not all hydrogens are shown. The enlarged atoms (except the Zn ion) are those used in calculation of the rmsd's presented in Figure 4. Color code: P, pink; C, gray; O, red; N, dark blue; S, yellow; Zn, light blue; H, white.

imidazole now acts as a hydrogen-bond donor via its His309-N$^{\epsilon}$H$^+$ moiety to the 2′-oxygen of Ado76. Indeed, this interaction is consistent in all five average structures. Furthermore, the average His309-**N**$^{\epsilon}$:···**O**-2′-Ado76 distance during the simulation is 2.97 Å. This is slightly shorter by 0.05 Å than that observed in the corresponding neutral bound active site (model **I**, 3.02 Å, see Figure 3) and, consequently, 0.34 Å shorter than in the X-ray crystallographic structure (PDB ID 1QF6).[20] Thus, protonation of His309 results in a strengthening of its interaction with Ado76.

As a consequence of this now reversed and strengthened His309···Ado76 interaction, in contrast to that observed in model **I**, the Ado76-2′-OH group is now able to act as a hydrogen-bond donor toward the phenolic oxygen of Tyr462. Furthermore, the Tyr462-**O**···**O**-2′-Ado76 distance has increased by 0.21 Å compared to model **I** to 3.09 Å. This indicates that the hydrogen bond between these two groups has weakened. Indeed, the Tyr462-**O**···**H**O-2′-Ado76 was not consistently maintained throughout the simulation. In fact, in approximately 43% of the conformers obtained the Ado76-2′-OH group formed an intramolecular hydrogen bond with the adjacent Ado76-3′-oxygen, i.e., Ado76-2′-O**H**···**O**-3′-Ado76. Thus, protonation of the imidazole of the His309 residue appears to weaken the interaction between the Tyr462-OH and the Ado76-2′-OH groups, which has been previously proposed to aid in stabilizing the fully bound active site.[21] In addition, in the fully bound active site model **I**−**H**$^+$ the Ado76-2′-oxygen is unlikely to act as a Brønsted base and deprotonate the Ado-3′-OH group.

In an acid-catalyzed aminoacyl transfer process the His309-N$^{\epsilon}$-H$^+$ proton could potentially transfer via the Ado-2′-OH and Ado-3′-OH groups onto the aminoacyl's carbonyl oxygen. This would enhance the electrophilicity of the adjacent carbonyl carbon (C1) and, in turn, its susceptibility to nucleophilic attack. However, from Figure 5 it can be seen that the Ado76-3′-OH does not consistently hydrogen bond to the carbonyl oxygen but rather to the Tyr462-OH group. Thus, it is unlikely that His309 would indirectly protonate the carbonyl oxygen. In addition, a mechanistically important geometric parameter is undoubtedly the distance between the Ado76-3′-oxygen and the C1 center of the threonyl moiety of the ThrAMP substrate. For model **I**−**H**$^+$, the average Ado76-3′**O**···**C1**-ThrAMP distance is 3.02 Å. Notably, this is 0.07 Å greater than that observed (2.95 Å) in the corresponding unprotonated fully bound active site model **I** (2.95 Å). Thus, protonation of the imidazole of the His309 residue appears to also negatively affect suitable positioning of the Ado76-3′-OH for nucleophilic attack at the threonyl's C1 center.

Effect of an Additional Active-Site Water on the Hydrogen Bonding Between His309-N$^{\epsilon}$ and Ado76-2′-OH. It has been alternatively suggested that an additional active-site water may act as a hydrogen-bond bridge between His309-N$^{\epsilon}$ and the Ado76-2′-OH group.[14] In order to examine this possibility, a water molecule was added to both models **I** and **I**−**H**$^+$ in the vicinity of His309-N$^{\epsilon}$ and Ado76-2′-OH,

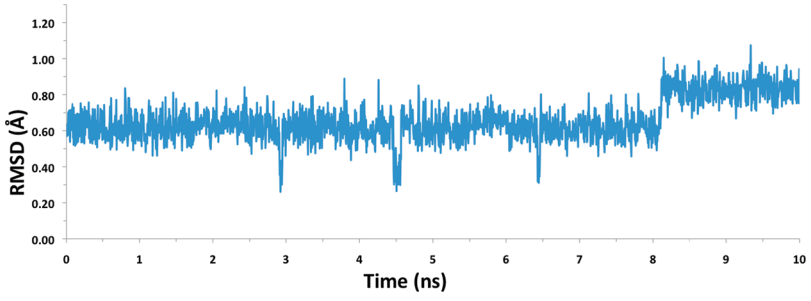

Figure 6. rmsd's in the positions of the His309 imidazole, phenol of Tyr462, ribose sugar ring of Ado76, threonyl moiety, and added bridging water molecule during the 10 ns simulation of model **II**.

dx.doi.org/10.1021/jp302556e | J. Phys. Chem. B 2012, 116, 5205−5212

generating models **II** and **II**−H^+ respectively (see Computational Methods).

For the fully bound active site containing an extra water but a neutral His309 residue, i.e., model **II**, the rmsd's for each conformation during the 10 ns period was determined based on the position of the His309 imidazole, Tyr462 phenol ring group, Ado76 ribose sugar, threonyl moiety, and added bridging water. The resulting values are shown plotted in Figure 6.

It can be clearly seen upon comparison with the rmsd's obtained for the corresponding model **I** (Figure 2) that introduction of the additional water significantly increases fluctuations in the positioning of the above moieties in the bound active site. In particular, at approximately 3.0, 4.5, and 6.5 ns in the collection period large, sudden, but short-lived deviations lasting just fractions of a nanosecond are observed with rmsd's decreasing by ∼0.3 Å. In addition, at approximately 8 ns a sudden, large increase in the rmsd's of ∼0.2 Å is observed lasting ∼2 ns. All these fluctuations in this rmsd profile reflect the intermittence of the hydrogen-bonding network of the bridging water molecule within the active site, and this contributes to disrupt the hydrogen-bonding network of Ado76.

The rmsd's were then subjected to a clustering analysis as per models **I** and **I**−H^+. Again, five clusters were produced and a representative average structure obtained for each. These structures are shown overlaid with each other in Figure 7 and

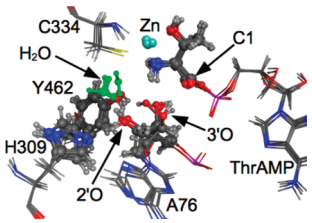

Figure 7. Overlay of the five representative average structures of model **II** obtained from cluster analysis of the rmsd's during the 10 ns MD simulation. For clarity, not all hydrogens are shown. The enlarged atoms (except the Zn ion) are those used in the calculation of the rmsd's presented in Figure 6. [Color code: P (pink); C (gray); O (red); N (dark blue); S (yellow); Zn (light blue); H (white); added H_2O (green)].

clearly show the greater variability in the relative positioning of the His309 imidazole, phenol of Tyr462, ribose sugar ring of Ado76, threonyl moiety, and bridging water molecule. Importantly, despite the average His309-**N**$^{\varepsilon}$···**O**-2′-Ado76 distance being quite long at 3.44 Å, at no time does it appear that the water inserts itself between His309 and Ado76-2′-OH. Instead, it prefers to sit to the side of both groups. As a consequence, the average Ado76-2′**O**···**O**H_2 distance is also markedly long at 2.75 Å while that for His309-**N**$^{\varepsilon}$···**O**H_2 is significantly even longer at 3.68 Å. This further suggests that any hydrogen-bonding interactions between H_2O and Ado76 or His309 are moderate or quite weak, respectively.

In comparison to that observed in models **I** and **I**−H^+, the Ado76-2′-OH group has markedly greater mobility. As a result, it alternates between acting as a hydrogen-bond donor with either the added H_2O moiety or the His309 imidazole N$^{\varepsilon}$ center. Inclusion of water was also found to negatively impact the interaction between the phenolic hydroxyl of Tyr462 and the Ado76-2′-OH groups. Indeed, while a Tyr462-O**H**···**O**-2′-Ado76 is consistently observed in all five average structures (Figure 7), the average Tyr462-**O**···**O**-2′-Ado76 distance has increased markedly by 0.38 Å (model **I**) to 3.26 Å. This suggests that while the interaction between these two groups is maintained, it has been notably weakened. In addition to resulting in less stabilization of the fully bound active site, this would also likely result in less stabilization of the "fully bound active site conformation" of the peptide loop containing Tyr462 (as noted in the Introduction).[21]

The above changes resulting from inclusion of water when His309 is neutral also negatively impacts the relative positioning of the mechanistically important Ado-3′-OH oxygen with respect to the threonyl's carbonyl carbon center (C1). Specifically, the average Ado-3′-**O**···**C1**═O distance has increased by 0.09 Å from that observed in model **I** (2.95 Å) to 3.04 Å in the present model **II**.

The effect of protonating the imidazole of His309 in the bound active site containing an additional water was then examined using model **II**−H^+. Alternatively, this can be thought of as considering the effects of adding a water to the His309-protonated bound active-site model **I**−H^+. As for the above model **II**, the rmsd's for each conformation during the 10 ns simulation (Figure 8) was determined based on the positions of the His309 imidazole, Tyr462 phenol, Ado76 ribose sugar, threonyl moiety, and added bridging water. In contrast to that observed for model **II**, no sudden, short- or long-lived fluctuations occur in the rmsd's. Instead, apart from the slightly higher fluctuations during the first nanosecond, they remain fairly consistent throughout the 10 ns simulation with most values lying between 0.9 ± 0.1 Å.

Again, a cluster analysis of the rmsd's was performed and a representative average structure obtained for each of the five resulting clusters. These are shown overlapped with each other in Figure 9. Similar to that seen for model **II**, i.e., neutral His309 with an added H_2O, the extra water in model **II**−H^+

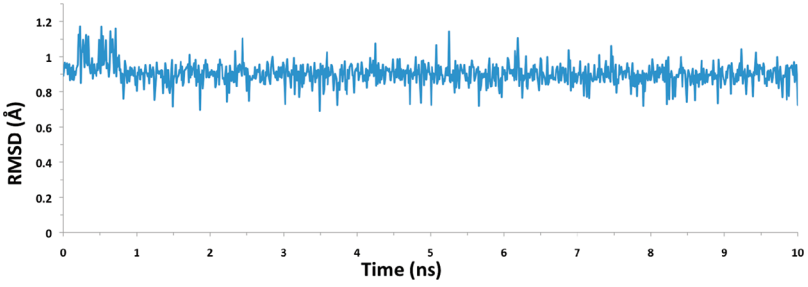

Figure 8. rmsd's in the positions of the His309 imidazole, phenol of Tyr462, ribose sugar ring of Ado76, threonyl moiety, and added bridging water molecule during the 10 ns simulation of model **II**−H^+.

dx.doi.org/10.1021/jp302556e | J. Phys. Chem. B 2012, 116, 5205−5212

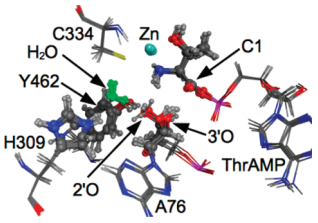

Figure 9. Overlay of the five representative average structures of model **II**–$\mathbf{H}^+$ obtained from cluster analysis of the rmsd's during the 10 ns MD simulation. For clarity, not all hydrogens are shown. The enlarged atoms (except the Zn ion) are those used in calculation of the rmsd's presented in Figure 8. Color code: P, pink; C, gray; O, red; N, dark blue; S, yellow; Zn, light blue; H, white; added H_2O, green.

does not bridge between His309-N^{ε} and the Ado76-2′-OH. In fact, the water instead appears to form a hydrogen-bonding bridge between His309-N^{ε} and the Ado76-3′-OH group. Indeed, the average His309-$\mathbf{N}^{\varepsilon}\cdots\mathbf{O}H_2$ and $H_2\mathbf{O}\cdots$**O**-3′-Ado76 distances are 2.84 and 3.24 Å, respectively. While the latter is 0.49 Å longer than the analogous $H_2\mathbf{O}\cdots$**O**-2′-Ado76 distance in model **II**, it is noted that the former (i.e., His309-$\mathbf{N}^{\varepsilon}\cdots\mathbf{O}H_2$) is markedly shorter by 0.84 Å than in model **II**. As a result, the added water appears to be better positioned to act as a bridge between the His309 residue's imidazole and the Ado76 nucleotidyl residue.

Importantly, as can be seen in Figure 9, the ribose ring of Ado76 has dramatically altered its position. In fact, its Ado76-2′-OH hydroxyl now hydrogen bonds with the carbonyl oxygen of the ThrAMP substrate with an average Ado76-2′-**O**$\cdots$**O**=C1 distance of 3.02 Å. Furthermore, the average distance between the mechanistically key Ado76-3′-OH oxygen and the threonyl's carbonyl carbon center has increased significantly by 0.5 Å to 3.53 Å. Thus, the combination of a protonated His309 residue and addition of a water disfavors nucleophilic attack by the Ado76-3′-oxygen at the Thr-AMP's C1 center.

In addition, it is noted that the proposed[21] important stabilizing Tyr462$\cdots$O-2′-Ado76 interaction has now been broken, with the Tyr462 phenolic hydroxyl instead hydrogen bonding with the Ado76-3′-OH group. The average distance for this latter interaction during simulations is 2.75 Å.

CONCLUSIONS

Molecular dynamics methods were used to investigate the structure of the fully bound active site of ThrRS for the second half-reaction, i.e., with both ThrAMP and $tRNA^{Thr}$ bound. In particular, the ability of His309 to act as either a mechanistic base (i.e., neutral) as proposed by Minajigi and Francklyn[14] or an acid (i.e., protonated) without or with the assistance of a bridging water was examined.

In the cases where His309 was protonated or unprotonated but with no additional bridging water added it was clearly seen that a stable interaction between His309 and Ado76 was formed.[14] Moreover, the Ado76-3′**O**$\cdots$**C1**-ThrAMP average distances of 2.95 and 3.02 Å in models **I** and **I**–$\mathbf{H}^+$, respectively, suggest that nucleophilic attack of C1 is possible for both protonation states. However, the +0.07 Å difference observed in **I**–$\mathbf{H}^+$ does suggest that protonation of His309 negatively affects suitable positioning of the Ado76-3′-OH for nucleophilic attack. Interestingly though, regardless of the protonation state of His309 it is unlikely that the Ado76-2′-oxygen would be able to deprotonate the adjacent Ado76-3′-OH group, allowing for nucleophilic attack of the C1 carbon of ThrAMP. Moreover, the possibility of an acid-catalyzed aminoacyl (i.e., indirect protonation of the carbonyl oxygen by His309) was also found to be unlikely. It is noted that in a recent cluster-DFT investigation we considered the involvement of His309 in the catalytic mechanism of ThrRS, and it was found that it did not act as the general base.[38]

Upon addition of a water molecule to bridge the His309-$\mathbf{N}^{\varepsilon}\cdots$**O**-2′-Ado76 interaction, for both the neutral and the protonated His309 significant disruptions to the orientation of the active-site groups are observed, that is, the current results suggest that an additional water does not bridge by hydrogen bonding between His309 imidazole and Ado76-2′-OH moieties regardless of the protonation state of His309. In addition, for neutral His309 it does not markedly affect the mechanistically important Ado76-3′-**O**$\cdots$**C1**=O distance (e.g., model **I** versus **II**). In contrast, for protonated His309, it causes significant distortions in the fully bound active-site conformation (e.g., model **II** versus **II**–$\mathbf{H}^+$). Therefore, a water is not necessary nor does it enhance positioning of the $tRNA^{Thr}$ cosubstrate for nucleophilic attack at the C1 center of the Thr-AMP substrate.

AUTHOR INFORMATION

Corresponding Author

*E-mail: gauld@uwindsor.ca.

Notes

The authors declare no competing financial interest.

ACKNOWLEDGMENTS

We thank the Natural Sciences and Engineering Research Council of Canada (NSERC), Canada Foundation for Innovation (CFI), the Ontario Innovation Trust (OIT), and SHARCNET for additional computational resources and graduate scholarships (W.J.H. and E.A.C.B.). E.A.C.B. also thanks NSERC for a PGS3D Scholarship. We thank C. S. Francklyn for helpful discussions.

REFERENCES

(1) Heinemann, I. U.; Jahn, M.; Jahn, D. *Arch. Biochem. Biophys.* **2008**, *474*, 238–251.
(2) Safro, M. G.; Moor, N. A. *Mol. Biol.* **2009**, *43*, 211–222.
(3) Cusack, S.; Berthetcolominas, C.; Hartlein, M.; Nassar, N.; Leberman, R. *Nature* **1990**, *347*, 249–255.
(4) Kisselev, L. L.; Favorova, O. O. *Adv. Enzymol. Relat. Areas Mol. Biol.* **1974**, *40*, 141–238.
(5) Mirande, M. *Prog. Nucleic Acid Res. Mol. Biol.* **1991**, *40*, 95–142.
(6) Schimmel, P. *Annu. Rev. Biochem.* **1987**, *56*, 125–158.
(7) Vasil'eva, I. A.; Moor, N. A. *Biochemistry-Moscow* **2007**, *72*, 247–263.
(8) Cusack, S. *Curr. Opin. Struct. Biol.* **1997**, *7*, 881–889.
(9) Arnez, J. G.; Moras, D. *Trends Biochem. Sci.* **1997**, *22*, 211–216.
(10) Uter, N. T.; Perona, J. J. *Biochemistry* **2006**, *45*, 6858–6865.
(11) Ibba, M.; Soll, D. *Annu. Rev. Biochem.* **2000**, *69*, 617–650.
(12) Malde, A. K.; Mark, A. E. *J. Am. Chem. Soc.* **2009**, *131*, 3848–3849.
(13) Liu, H. N.; Gauld, J. W. *J. Phys. Chem. B* **2008**, *112*, 16874–16882.
(14) Minajigi, A.; Francklyn, C. S. *Proc. Natl. Acad. Sci. U.S.A.* **2008**, *105*, 17748–17753.
(15) Pyrkosz, A. B.; Eargle, J.; Sethi, A.; Luthey-Schulten, Z. *J. Mol. Biol.* **2010**, *397*, 1350–1371.
(16) Liu, H. N.; Gauld, J. W. *J. Phys. Chem. B* **2008**, *112*, 16874–16882.
(17) Guth, E.; Connolly, S. H.; Bovee, M.; Francklyn, C. S. *Biochemistry* **2005**, *44*, 3785–3794.

(18) Dock-Bregeon, A. C.; Sankaranarayanan, R.; Romby, P.; Caillet, J.; Springer, M.; Rees, B.; Francklyn, C. S.; Ehresmann, C.; Moras, D. *Cell* **2000**, *103*, 877−884.
(19) Sankaranarayanan, R.; Dock-Bregeon, A. C.; Rees, B.; Bovee, M.; Caillet, J.; Romby, P.; Francklyn, C. S.; Moras, D. *Nat. Struct. Biol.* **2000**, *7*, 461−465.
(20) Sankaranarayanan, R.; Dock-Bregeon, A. C.; Romby, P.; Caillet, J.; Springer, M.; Rees, B.; Ehresmann, C.; Ehresmann, B.; Moras, D. *Cell* **1999**, *97*, 371−381.
(21) Torres-Larios, A.; Sankaranarayanan, R.; Rees, B.; Dock-Bregeon, A. C.; Moras, D. *J. Mol. Biol.* **2003**, *331*, 201−211.
(22) Llano, J., Gauld, J. W. In *Quantum Biochemistry: Electronic Structure and Biological Activity*; Matta, C. F., Ed.; Wiley-VCH: Weinheim, 2010; Vol. 2, pp 643−666.
(23) Archontis, G.; Simonson, T.; Karplus, M. *J. Mol. Biol.* **2001**, *306*, 307−327.
(24) Bharatham, N.; Bharatham, K.; Lee, Y.; Lee, K. W. *Biophys. Chem.* **2009**, *143*, 34−43.
(25) Budiman, M. E.; Knaggs, M. H.; Fetrow, J. S.; Alexander, R. W. *Proteins* **2007**, *68*, 670−689.
(26) Hansia, P.; Ghosh, A.; Vishveshwara, S. *Mol. Biosyst.* **2009**, *5*, 1860−1872.
(27) Hughes, S. J.; Tanner, J. A.; Miller, A. D.; Gould, I. R. *Proteins* **2006**, *62*, 649−662.
(28) Kapustina, M.; Carter, C. W. *J. Mol. Biol.* **2006**, *362*, 1159−1180.
(29) Sethi, A.; Eargle, J.; Black, A. A.; Luthey-Schulten, Z. *Proc. Natl. Acad. Sci. U.S.A.* **2009**, *106*, 6620−6625.
(30) Thompson, D.; Lazennec, C.; Plateau, P.; Simonson, T. *Proteins* **2008**, *71*, 1450−1460.
(31) Yamasaki, S.; Nakamura, S.; Terada, T.; Shimizu, K. *Biophys. J.* **2007**, *92*, 192−200.
(32) *MOE*, 2009.10 ed.; Chemical Computing Group Inc.: Montreal, Quebec, Canada, 2009.
(33) Sekine, S.; Nureki, O.; Dubois, D. Y.; Bernier, S.; Chenevert, R.; Lapointe, J.; Vassylyev, D. G.; Yokoyama, S. *EMBO J.* **2003**, *22*, 676−688.
(34) Bond, S. D.; Leimkuhler, B. J.; Laird, B. B. *J. Comput. Phys.* **1999**, *151*, 114−134.
(35) Nelson, D. L.; Cox, M. M. *Lehninger: Principles of Biochemistry*, 4th ed.; W. H. Freeman and Co.: New York, 2005.
(36) Bushnell, E. A. C.; Erdtman, E.; Llano, J.; Eriksson, L. A.; Gauld, J. W. *J. Comput. Chem.* **2011**, *32*, 822−834.
(37) Banas, P.; Walter, N. G.; Sponer, J.; Otyepka, M. *J. Phys. Chem. B* **2010**, *114*, 8701−8712.
(38) Huang, W. J.; Bushnell, E. A. C.; Francklyn, C. S.; Gauld, J. W. *J. Phys. Chem. A* **2011**, *115*, 13050−13060.